Journal of Ceramic Processing Research. Vol. 12, No. 3, pp. 259~264 (2011)

J O U R N A L O F
Ceramic Processing Research

ZrO_2 and Y_2O_3-stablized ZrO_2 coatings deposited using an arc ion plating technique

Qi Min Wang[a,b,*], Jun Gong[a], Chao Sun[a], Hyung Woo Lee[b] and Kwang Ho Kim[b,*]

[a]*Division of Surface Engineering Materials, Institute of Metal Research, 72 Wenhua Road, Shenyang, P.R. China*

[b]*National Core Research Center for Hybrid Materials Solution, Pusan National University, Busan 609-735, South Korea*

ZrO_2 and Y_2O_3-stablized ZrO_2 (YSZ) coatings were deposited on NiCoCrAlY coated superalloys using an arc ion plating system. The crystalline structure, chemical composition, and morphology of the coatings were systematically investigated using X-ray diffraction, X-ray photoelectron spectroscopy, as well as scanning electron microscopy. The thermal stability of YSZ coatings were investigated by oxidation and thermal shock tests. The results showed that near-stoichiometric ZrO_2 coatings can be obtained at a relatively large range of O_2 flow rates (134-400 sccm), with the main phase of monolithic zirconia being identified. YSZ coatings exhibited excellent thermal stability in the oxidation and thermal shock tests. Before and after thermal tests, only the tetragonal zirconia (t-ZrO_2) phase was identified in the YSZ coatings.

Key words: ZrO_2 coating, Arc ion plating, Phase structure,; Thermal stability, Thermal shock resistance.

Introduction

Zirconium oxide (ZrO_2) exhibits excellent properties as a ceramic material, such as low thermal conductivity, excellent corrosion resistance, high ionic conductivity, and good optical properties (high refractive index, low absorption, and weak loss from near-ultraviolet to mid infrared). This makes it of interest for a wide range of coating applications, including thermal barrier coatings (TBCs), wear-resistant coatings, optical films, substrate buffer layers, and as a solid electrolyte in solid oxide fuel cells (SOFC) [1-5].

ZrO_2 exists in three crystallographic phases: a monoclinic phase at low temperature, a tetragonal phase at intermediate temperatures and a cubic phase at high temperature. In particular, the phase transformation from the tetragonal phase to the monoclinic phase is accompanied by a significant volume expansion (approximately 3~5 vol %), which results in cracking and contributes to the failure of ZrO_2 material [6, 7]. Therefore, in the case of thick coatings, such as TBCs, a tetragonal phase stabilizer (e.g., Y_2O_3, CeO_2, MgO) is added to repress the detrimental phase transformation. The most widely used stabilizer is Y_2O_3. Y_2O_3-stabilized ZrO_2 (YSZ) coatings have been widely applied as the topcoat of thermal barrier coatings [1].

A variety of techniques have been utilized to synthesize ZrO_2 and ZrO_2-based coatings, such as magnetron sputtering [6, 8], ion-assisted deposition [9], plasma spraying [10, 11], electron-beam physical vapor deposition (EB-PVD) [12] and chemical vapor deposition (CVD) techniques [13]. Arc ion plating possesses the merits of being able to produce crystalline ceramic films at low deposition temperatures due to the very high percentage of vapor ionization and the high kinetic energy of the emitted ions [14-17]. Also, its high deposition rate, strong film adhesion, ability to uniformly cover complex shaped components, and low manufacturing cost makes it very attractive to produce zirconia-based coatings to be used as TBCs, in fuel cells and gas sensors, etc. Up to date, very few reports have been involved in ZrO_2-based coatings deposited using an arc ion plating technique. In particular, there is no report of YSZ coatings deposited by an arc ion plating technique as the topcoat of thermal barrier coatings.

In the present study, we deposited ZrO_2 and Y_2O_3-stablized ZrO_2 (YSZ) coatings using an arc ion plating system. The phase structure and thermal stability of ZrO_2 and YSZ coatings were investigated. An arc ion plated YSZ coating as the topcoat of a thermal barrier coating was attempted.

Experimental Details

The Ni32Co20Cr8Al0.5Y (wt. %) coated IN100 superalloy pieces (C 0.15, Cr 8.7, Co 14.5, Mo 2.8, Al 5.2, Ti 4.6, V 0.83, Fe 0.6, and balanced Ni, wt. %) were used as the substrates. The depositing parameters of the NiCoCrAlY coatings on IN100 substrates are similar to that reported in reference [18]. The thickness of the NiCoCrAlY coatings were about 20-40 μm. Some sheets with a thickness of 100-200 μm were prepared by stripping most of the IN100 superalloy substrates from the NiCoCrAlY coated specimens by grinding. These sheets were also coated with zirconium oxide in order to obtain the fractured cross-sections of coatings.

Coatings were deposited in an arc ion plating equipment (AIP-10-1300). The cathode was pure Zr (> 99.9 wt %) or Zr-8Y (wt %). After the base pressure in the chamber was

*Corresponding author:
Tel : +82-51-510 3796
Fax: +82-51-518 3360
E-mail: qmwang@imr.ac.cn(Q.M. Wang),
kwhokim@pusan.ac.kr(K.H. Kim)

below 6×10^{-3} Pa, bombardment cleaning and the subsequent deposition process were carried out. The working pressure was kept at 7×10^{-2} Pa by flowing argon into the chamber during bombardment cleaning. Then the zirconium oxide and YSZ coatings were fabricated by evaporation of the cathodes in an uninterrupted supply of oxygen (or a mixed gas of oxygen and argon). The deposition parameters are shown in Table 1. Isothermal oxidation tests were conducted in static air at 900 °C and 1000 °C in alumina crucibles placed in a muffle furnace. The oxidation time was 5 h. Thermal shock tests were conducted in a thermal cycling furnace. Each cycle consisted of directly inserting samples at 1100 °C, followed by 10 minutes holding them at 1100 °C, and then plunging them in water (room temperature, 20-30 °C).

The deposition rates of coatings were measured from the polished cross-sectional images. Characterizations of the surface and cross-section morphologies of the ZrO_2 and YSZ coatings were carried out using scanning electron microscopy (SEM, JSM -6301F). The phase structures of the coatings were studied by X-ray diffraction (XRD, D/max-RA), using standard Bragg-Brentano geometry with Cu-K_α radiation. The scanning speed was 0.2°minute^{-1}. The average crystallite size D of the coatings was estimated using the Scherrer equation: $D = 0.9\lambda/(\beta \cos\theta)$, where λ is the X-ray wavelength, θ the diffraction angle and β the full width of peak at half maximum intensity (FWHM) [19]. X-ray photoelectron spectroscopy (XPS) employing an ESCALAB250 surface analysis system was utilized to determine the chemical composition and bond status of the ZrO_2 and YSZ coatings. The samples were analyzed after etching with a 4 keV Ar^+ ion beam for 10 minutes to reduce surface contamination.

Results and Discussion

Deposition of ZrO_x coatings

In a reactive arc ion plating process, the working status of the cathode is affected significantly by the partial pressure of the reactive gas. Fig. 1(a) outlines the specific machine parameters (arc voltage and arc current) influenced by the flux rate of oxygen (oxygen partial pressure). An apparent increase in arc voltage and decrease in arc current can be seen with an increase in the oxygen partial pressure. This phenomenon was found to be more serious after a longer deposition time. The reason lay in the "target poisoning effect" [20], i.e. the surface of the Zr cathode being partly covered by oxides of Zr. When target poisoning occurred, the electrical and physical characters of the target changed significantly, thereby affecting the working status of the cathode (e.g., density and motivation of arc spots, arc voltage, etc.). Fig. 1(b) shows the deposition rate of ZrO_2 coating as a function of the flux rate of oxygen. The reduction in the deposition rate at a higher flux rate of oxygen should also be attributed to target poisoning. The evaporation rate of Zr oxide is lower than that of pure Zr metal due to much the higher melting point of

Table 1. Deposition parameters of ZrO_x and Y_2O_3-stablized ZrO_2 (YSZ) coatings using an arc ion plating technique

	ZrO_x coating	YSZ coating
Cathode target	Zr (> 99.9 wt %)	Zr-8Y (wt %)
Flow rate of O_2 (sccm)	80-400	134-300
Chamber pressure (Pa)	0.8	0.6-1.2
Arc voltage (V)	18-35	18-40
Arc current (A)	84-95	50-60
Bias voltage (V)	-300	-300
Bias duty cycle	30%	30%
Temperature (°C)	200-300	300-400
Substrate ratation	No	Yes
Coatings time (h)	0.5-1	5

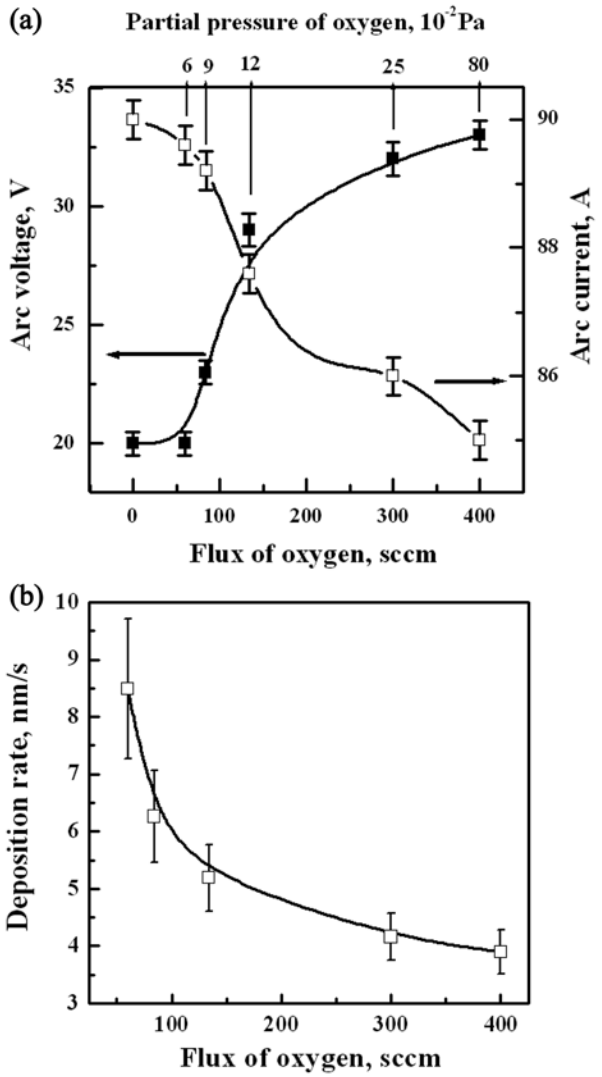

Fig. 1. (a) Variations of the arc voltage and current with the varying fluxing rate of oxygen during the deposition of ZrO_2 coatings (the values were recorded after coating deposition for 5 minutes); (b) Deposition rate of ZrO_2 coating versus flow rates of oxygen.

Zr oxide than that of pure Zr. Therefore, a dramatic voltage increase, a significant decrease in deposition rate, and an uncontrolled increase in processing pressure can result from target poisoning. To obtain a stable deposition, a high oxygen partial pressure should be avoided.

The chemical composition of the zirconia coatings as a function of the flux rate of oxygen are shown in Fig. 2(a). With an increase in the flux rate of oxygen from 80 sccm to 400 sccm, the O concentration in the coatings increased from 59 at.% to 64 at.%. The Zr atomic ratio decreased from 41 at.% to 36 at.%, and hence, the elemental ratio of O to Zr increased from 1.44 to 1.78. Near-stoichiometric films were obtained at a flux rate of oxygen of 134-400 sccm. Fig. 2(b) shows XPS spectra of Zr *3d* of zirconia coatings deposited at various flux rates of oxygen. Each spectrum was fitted by a least-squares method using a Gaussian-Lorentzian envelope. The main chemical state in the coatings was Zr^{4+} [21], with the Zr $3d_{3/2}$ and Zr $3d_{5/2}$ subpeaks being centered at 185.3 ± 0.2 eV and 182.9 ± 0.2 eV, respectively.

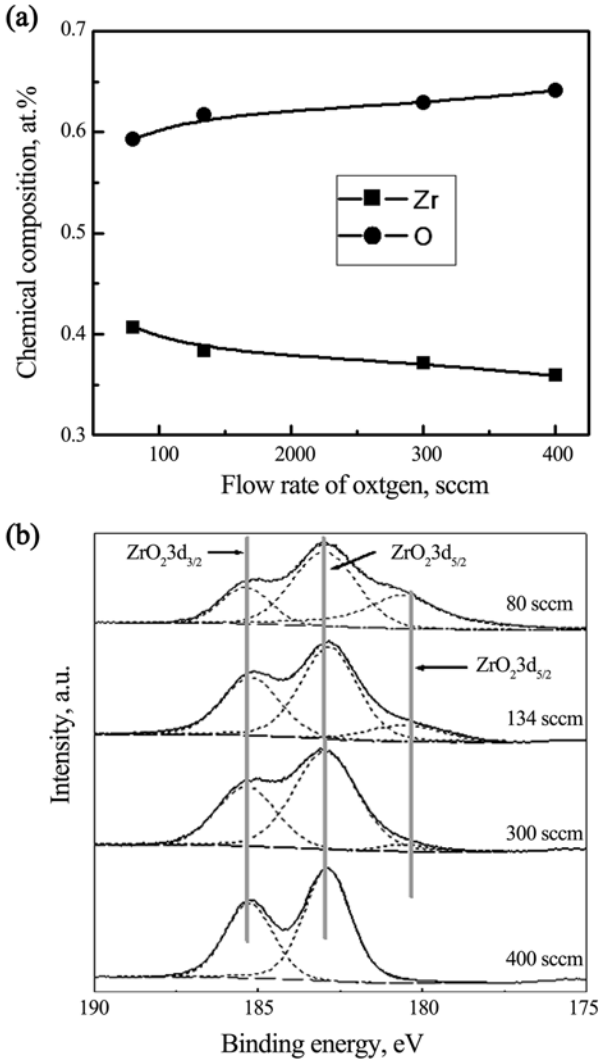

Fig. 2. (a) Chemical composition of ZrO_2 coatings versus flow rates of oxygen; (b) XPS spectra of Zr *3d* of ZrO_2 coatings deposited at various flux rates of oxygen.

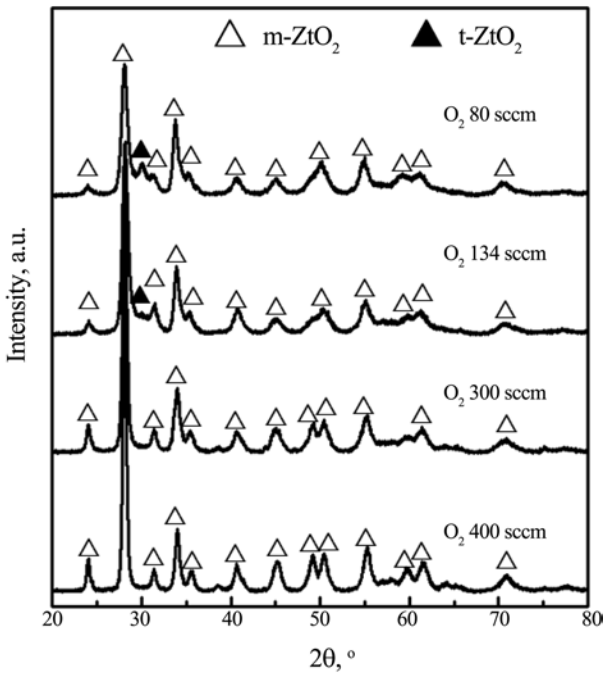

Fig. 3. XRD patterns of ZrO_2 coatings deposited at various flux rates of oxygen.

Another sub-peak centered at 180.5 ± 0.2 eV also appeared at a low oxygen partial pressure. This peak can be attributed to ZrO_x $3d_{5/2}$ (x < 2), i.e. the suboxidation states of Zr (Zr^{3+}, Zr^{2+}, Zr^{+}) or metallic Zr (Zr^0). Corresponding to the chemical compositions in Fig. 2(a), the intensity of ZrO_x $3d_{5/2}$ sub-peak decreased apparently with an increase of the flux rate of oxygen. Complete oxidation of Zr was obtained in the films at a high oxygen partial pressure.

Fig. 3 shows XRD results for the ZrO_x coatings deposited at different O_2 flow rates. Almost all the diffraction peaks can be attributed to monoclinic zirconia (m-ZrO_2) phase. At an oxygen flow rate of 80 sccm, a peak of the tetragonal zirconia (t-ZrO_2) phase appeared at ~29.7°. This peak disappeared at O_2 flow rates higher than 134 sccm. In other references, it was also found that oxygen-deficient ZrO_2 may contain the metastable t-ZrO_2 phase [22, 23]. Fig. 4 shows typical surface and cross-sectional SEM morphologies of zirconia coatings. Formation of dense columns was observed along the growth direction. Round tops were on the top of columns. The zirconia films have similar undulations as the underneath NiCoCrAlY coatings. From the fractured cross sectional images, it was revealed that the zirconia films consist of fine columns with a feathery structure.

YSZ coatings on NiCoCrAlY coated superalloy substrates

From the above results, it seems that near-stoichiometric ZrO_2 coatings can be obtained at a relatively wide range of O_2 flow rates (134-400 sccm). By using deposition parameters of ZrO_2 coatings as references, we synthesized YSZ coatings using arc ion plating. The YSZ coatings

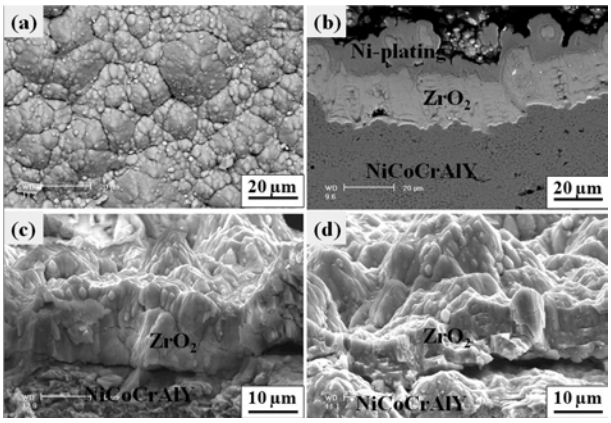

Fig. 4. Surface (a), polished cross-sectional (b), and fractured cross-sectional (c, d) SEM images of ZrO_2 coatings on NiCoCrAlY coated IN 100 specimens deposited by arc ion plating. (a, b, c) O_2 134 sccm; (d) O_2 300 sccm.

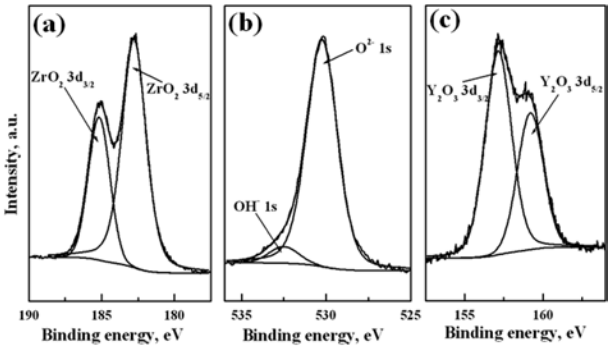

Fig. 5. XPS spectra of YSZ coating deposited by arc ion plating. (a) Zr *3d*; (b) Y *3d*; (c) O *1s*.

were deposited by evaporation of the ZrY target in an oxygen flow of 134-300 sccm. The total pressure of O_2 + Ar was 0.6-1.2 Pa. To investigate the possibility of YSZ coatings as the topcoat of thermal barrier coatings, we deposited the YSZ coatings on NiCoCrAlY coated IN100 substrates and investigated them in high-temperature oxidation and thermal shock tests.

From the XPS results, the chemical composition of the YSZ coating deposited by arc ion plating was: 24.6 at.% Zr, 9.1 at.% Y, and 66.3 at.% O, corresponding to an Y_2O_3 molar fraction of about 16%. Fig. 5 shows XPS spectra of Zr *3d*, O *1s*, and Y *3d* of an arc ion plated YSZ coating. The Zr *3d* and Y *3d* binding energies are in good agreement with those of Zr^{4+} and Y^{3+} in ZrO_2 and Y_2O_3, respectively [24]. No suboxidation states of Zr (Zr^{3+}, Zr^{2+}, Zr^{+}) or metallic Zr (Zr^0) were observed in the Zr *3d* spectrum. In the O *1s* spectrum, the main chemical state corresponded to O^{2-} in the ZrO_2 or Y_2O_3. A small peak corresponding to OH^- at a high binding energy was also detected, which might come from surface contamination.

Fig. 6(a) and Fig. 6(b) show surface and cross sectional SEM images of arc ion plated YSZ coatings in the as-deposited condition. Feather-like tops were observed on the coating surface, with macroparticles and discharge remains being detected in some areas. The coating was

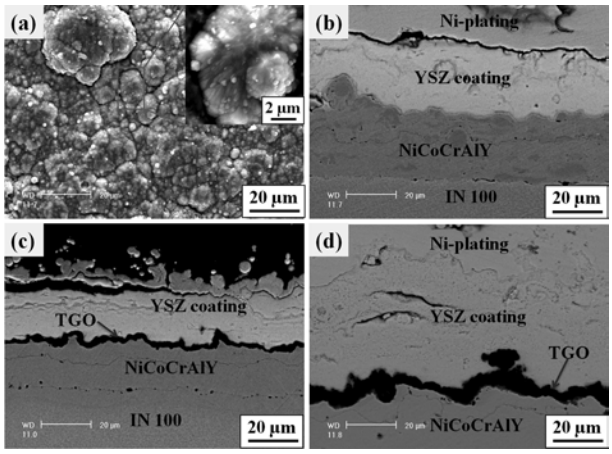

Fig. 6. Surface (a) and polished cross-sectional (b, c, d) SEM images of YSZ coatings on NiCoCrAlY coated IN 100 specimens. (a, b) As-deposited coating; (c) After oxidation at 1000 °C for 5 h; (d) After 50 cycles of 1100 °C RT.

very dense and well adhered to the NiCoCrAlY coating. After oxidation at 1000 °C for 5 h, the YSZ/NiCoCrAlY/IN 100 specimen remained almost intact. From the cross-sectional SEM image in Fig. 6(c), a thermally grown oxide (TGO) layer formed at the YSZ/NiCoCrAlY interface may be seen. The TGO layer was formed by the oxidation of the NiCoCrAlY coating beneath the YSZ coating layer, which was oxygen transparent. EDX results revealed that the TGO layer was mainly of Al_2O_3. After the thermal shock test, the coated specimen was still perfect in most regions, except some damage was detected in specimen edges/corners. Fig. 6d shows the cross-sectional SEM image of a YSZ/NiCoCrAlY/IN 100 specimen after 50 thermal shock cycles of 1100 °C → room temperature (RT). The coated specimen exhibited very good thermal shock resistance. No cracks or delimitations were observed. Also a TGO layer mainly of Al_2O_3 was detected between the YSZ coating and the NiCoCrAlY coating. The TGO layer in Fig. 6d is thicker than that in Fig. 6(c).

Fig. 7 shows XRD results of YSZ coatings on NiCoCrAlY coated IN100 specimens in the as-deposited condition and after the oxidation and thermal shock tests. Only the tetragonal zirconia phase was identified in the YSZ coating. Very weak γ-Ni peaks were also detected, which might originate from the NiCoCrAlY coating underneath. After oxidation or thermal shock tests, no monoclinic ZrO_2 phase was detected, which has often been observed due to degradation of the YSZ overcoat in the TBCs after high-temperature oxidation or thermal shock tests [25, 26]. Therefore, it can be concluded that no phase degradation occurred in the YSZ coatings during the oxidation and thermal shock tests. The only detected change was the apparent broadening of XRD peaks in the as-deposited condition and much narrower peaks after the oxidation and thermal shock tests. Table 2 shows the FWHM of the (003) peaks (~29.7°) of the t-ZrO_2 phase in the YSZ coatings before and after the oxidation and thermal shock

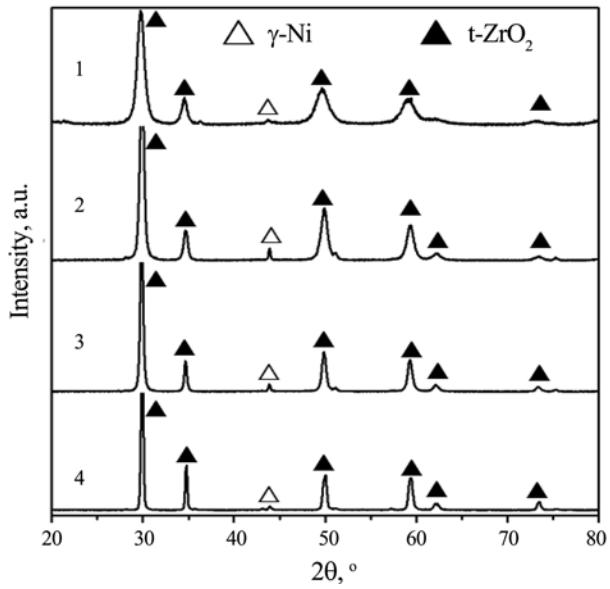

Fig. 7. XRD patterns of YSZ coatings on NiCoCrAlY coated IN100 specimens. 1: as-deposited coating; 2: after oxidation at 900 °C for 5 h; 3: after oxidation at 1000 °C for 5 h; 4: after 50 cycles of 1100 °C RT.

Table 2. FWHM of the (003) peaks (~29.7°) of the t-ZrO_2 phase in Fig. 7 and the grain size values calculated using the Scherrer equation

Specimens	FWHM (°)	Grain size (nm)
As-deposited	0.897	10.0
900 °C, 5 h	0.527	17.0
1000 °C, 5 h	0.396	22.6
50 thermal cycles (1100 °C RT)	0.339	26.4

tests and the crystallite sizes calculated using the Scherrer equation. It can be seen that the YSZ coating deposited by arc ion plating possessed a nano-sized microstructure with an average grain size of about 10.0 nm. During the process of the oxidation and thermal shock tests, the crystallite size increased. After oxidation at 900 °C for 5 h, the average crystallite size increased to 17.0 nm. After 10 h at 1000 °C and 50 cycles of 1100 °C RT, the values increased to 22.6 nm and 26.4 nm, respectively. The arc ion plating process is a far-from-equilibrium process, during which impinging high-energy particles (ions, neutral atoms, and atom clusters or macroparticles) deposit on the substrates at an extremely fast cooling rate [27]. Therefore, the as-deposited YSZ coating exhibited a nanocrystalline microstructure. In the high-temperature annealing, coalescence of nanocrystals and recrystallization occurred, which resulted in an increased crystallite size after the oxidation or thermal shock tests.

The results in this study revealed that arc ion plated YSZ coatings have the potential to be used as thermally insulative topcoats in thermal barrier coatings. Firstly, high-energy ion bombardment during the coating deposition can remove the absorbed gases and impurities on the specimen surface and improve the coating-substrate adherence. In this study, good adherence between the YSZ coatings and the NiCoCrAlY coatings underneath was observed in the specimens before and after the oxidation and thermal shock tests (Fig. 6). Secondly, the nanocrystalline YSZ coatings deposited exhibited excellent thermal shock resistance in this study. Lastly, coating formation species in the arc ion plating process are high ionization (> 80-90%) species with high-energy ions from the arc discharge, which are in favor of compound formation. In this study, near-stoichiometric ZrO_2 coatings and YSZ coatings composed of the tetragonal zirconia phase could be obtained at a relatively large range of O_2 flow rates (134-300 sccm). Such a large window of deposition parameters are favorable industrialization.

However, the present study is not a real investigation on fabricating an YSZ coating as the topcoat of TBCs. The arc ion plated YSZ coating in this study is too thin, only 20-40 μm as compared to 200-400 μm in normal TBCs. Several weaknesses, such as increasing the coating thickness by increasing the deposition rate and solving the problems of substrate arcing and target poisoning, have to be conquered before the arc ion plated YSZ coatings can be applied as the topcoat of TBCs in industry.

Conclusions

(1) Zirconium oxide coatings were deposited at various oxygen inlet flux rates using an arc ion plating system. Near-stoichiometric ZrO_2 coatings could be obtained at a relatively large range of O_2 flow rates (134-400 sccm). The phase in the coatings was mainly monoclinic zirconia (m-ZrO_2).

(2) YSZ coatings were deposited on NiCoCrAlY coated IN100 substrates. The coatings exhibited excellent thermal stability during high-temperature oxidation and thermal shock tests. Before and after the thermal tests, only the tetragonal zirconia (t-ZrO_2) phase was identified in the YSZ coatings. An increase of the crystallite size was detected in the high-temperature exposure.

Acknowledgements

Qi Min Wang acknowledgements financial supports from the National Science Foundation of China under grant No. 50701046. Kwang Ho Kim acknowledges financial support from NCRC (National Core Research Center) program through the National Research Foundation of Korea funded by the Ministry of Education, Science and Technology (2010-0001-226).

References

1. N.P. Padture, M. Gell and E.H. Jordan, Science 296[5566] (2002) 280-284.
2. J.T. Chang, C.H. Yeh, J.L. He, K.C. Chen, A. Matthews and A. Leyland, Surf. Coat. Technol. 200[5-6] (2005) 1401-1406.
3. V.V. Kharton, F.M.B. Marques and A. Atkinson, Solid

State Ionics 174[1-4] (2004) 135-149.
4. Q. Xiao, H. He, S. Shao, J. Shao and Z. Fan, Thin Solid Films 517[15] (2009) 4295-4298.
5. O. Kazuhito and K. Sato, J. Ceram. Process. Res. 3[3] (2002) 114-117.
6. P. Briois, F. Lapostolle, V. Demange, E. Djurado and A. Billard, Surf. Coat. Technol. 201[12] (2007) 6012-6018.
7. J. Moon, H. Choi and C. Lee, J. Ceram. Process. Res. 1[1] (2000) 69-73.
8. P.T. Gao, L.J. Meng, M.P. dos Santos, V. Teixeira and M. Andritschky, Thin Solid Films 377-378 (2000) 557-561.
9. M.G. Krishna, K. Rao and S. Mohan. Thin Solid Films 207[1-2] (1992) 248-251.
10. K. Brinkiene and R. Kezelis, J. Euro. Ceram. Soc. 24[6] (2004) 1095-1099.
11. O. Kwon, S. Kumar, S. Park and C. Lee, J. Ceram. Process. Res. 10[2] (2009) 139-143.
12. D.E. Wolfe, J. Singh, R.A. Miller, J.I. Eldridge and D.-M. Zhu, 190[1] (2005) 132-149.
13. V.G. Varanasi, T.M. Besmann, R.L. Hyde, E.A. Payzant and T.J. Anderson, J. Alloys Comp. 470[1/2] (2009) 354-359.
14. A. Anders, Vacuum 67[3-4] (2002) 673-686.
15. A.L. Ji, W. Wang, G.H. Song, Q.M. Wang, C. Sun and L.S. Wen, Mater. Lett. 58[14] (2004) 1993-1998.
16. H.J. Kim, J.J. Kim, K.B. Kim and G.S. Lee, J. Ceram. Process. Res. 10[4] (2009) 473-476.
17. J.S. Yun, Y.S. Hong, K.H. Kim, S.H. Kwon and Q.M. Wang, J. Korean. Phys. Soc. 57[1] (2010), in press.
18. Q.M. Wang, Y.N. Wu, P.L. Ke, H.T. Cao, J. Gong, C. Sun and L.S. Wen, Surf. Coat. Technol. 186[3] (2004) 389-397.
19. H.P. Klug and L.E. Alexander, in "X-ray diffraction procedures for polycrystalline and amorphous materials" (2nd ed., John Wiley & Sons, New York, 1974) p. 656.
20. I. Safi, Surf. Coat. Technol. 127[2-3] (2000) 203-218.
21. T.M. Grehk, J. Engkvist, U. Bexell, J.H. Richter, P.G. Karlsson and A. Sandell, Thin Solid Films 516[6] (2008) 875-879.
22. T.G. Kuznetsova and V.A. Sadykov, Kinetics and Catalysis 49[6] (2008) 840-858.
23. J.P. Holgado, J.P. Espinós, F. Yubero, A. Justo, M. Ocaña, J. Benítez and A.R. González-Elipe, Thin Solid Films 389[1-2] (2001) 34-42.
24. F. Parmigiani, L.E. Depero, L. Sangaletti and G. Samoggia, J Electron. Spectrosc. Relat. Phenom. 63[1] (1993) 1-10.
25. S.A. Tsipas, J. Euro. Ceram. Soc. 30[1] (2010) 61-72.
26. P.L. Ke, Y.N. Wu, Q.M. Wang, J. Gong, C. Sun and L.S. Wen, 200[7] (2005) 2271-2276.
27. L.S. Wen and R.F. Huang, Surf. Coat. Technol. 193[1-3] (2005) 1-5.